

# A Nonaxisymmetric Endwall Design Approach and Its Computational Assessment in the NGV of an HP Turbine Stage

Ozhan H. Turgut<sup>1</sup>

*Praxair Inc., Tonawanda, NY, 14150*

Cengiz Camci<sup>2</sup>

*The Pennsylvania State University, University Park, PA, 16802*

**Nonaxisymmetric endwall contouring has recently become one of the ways to minimize the secondary flow related losses in a turbine nozzle guide vane (NGV) passage. In this study, a specific nonaxisymmetric endwall contouring design methodology is introduced. Fourier series based splines at different axial locations are generated and combined with the help of streamwise B-splines within solid modeling program. Eight different contoured endwalls are presented in this paper. Computational study of these designs are performed by the finite-volume flow solver. The SST k- $\omega$  turbulence model is selected and a bodyfitted structured grid is used. Total pressure distribution at the NGV exit shows that contouring the endwall effectively changes the results. Among from these various designs, the most promising one is with the contouring extended in the upstream of the vane leading edge. Mass-averaged value of 3.2% total pressure loss reduction is achieved at the NGV exit plane. The current study was performed in a rotating turbine rig simulating a state of the art HP turbine stage. An NGV only simulation is performed. This approach is helpful in isolating rotor-stator influence and the possible upstream flow modifications of the rim seal cavity flow existing in the rotating turbine research rig. The investigation including the rotor-stator interaction and rim seal cavity flow is the topic of a subsequent paper currently under progress.**

---

<sup>1</sup> Development Specialist, Turbomachinery Aerodynamics, 175 East Park Dr., Tonawanda NY 14150.

<sup>2</sup> Professor of Aerospace Engineering, ASME Fellow, 223 Hammond Bldg., University Park PA 16802.

## Nomenclature

$a, b$	= Fourier series coefficients
$c$	= Midspan axial chord length of nozzle guide vane
$C_p$	= Static pressure coefficient, $\frac{P_1 - P_2}{0.5 \rho U_m^2}$
$C_{pt}$	= Total pressure coefficient, $\frac{P_{02} - P_{01}}{0.5 \rho U_m^2}$
$k$	= Turbulence kinetic energy
$K$	= Scaling coefficient
$L$	= Circumferential distance between reference points
$p$	= Circumferential distance between two blades
$P$	= Static pressure
$P_0$	= Total pressure
$r$	= Radius, radial direction
$Re_{\theta t}$	= Momentum-thickness Reynolds number
$U_m$	= Blade speed at mean radius
$V$	= Velocity magnitude
$V_\theta$	= Circumferential velocity component
$x, y, z$	= Cartesian coordinates for computations (x also for axial direction)
$y^+$	= Non-dimensional wall coordinate, $\frac{\sqrt{\tau_w/\rho} \cdot y_p}{\nu}$
$y_p$	= First grid height off the wall
$\gamma$	= Intermittency
$\theta$	= Circumferential direction
$\nu$	= Kinematic viscosity
$\rho$	= Density
$\tau_w$	= Wall shear stress
$\omega$	= Turbulent frequency
1	= One axial chord upstream of nozzle guide vane leading edge

$2$  = Nozzle guide vane exit plane,  $\frac{x}{c} = 1.025$

$N$  = Turbine nozzle guide vane

$R$  = Turbine rotor blade

$SST$  = Shear stress transport

$TKE$  = Turbulence kinetic energy

## I. Introduction

The history of the nonaxisymmetric endwall contouring dates back to mid 1970's. Until now, various methods are utilized to design contoured endwalls. These methods can be classified mainly as:

- Cubic convergence profiles in a plane orthogonal to the streamwise direction,
- Convex curvature design (creating bump close to either pressure surface or suction surface),
- Sinusoidal curve in circumferential direction and parametric curve in axial direction,
- Fourier series curve in circumferential direction and B-Splines along axial direction,
- Half cosine wave in circumferential direction and offsetting blade camber line vertically in axial direction,
- Multiplication of the two parameterized functions, one in circumferential direction and the other in axial direction,
- 2D cubic splines both in circumferential direction and streamwise direction.

Morris and Hoare [1] conducted linear cascade experiments with meridional and nonaxisymmetric endwall profiling. Their nonaxisymmetric profile is the same as the axisymmetric one except that the span-width contours of the profile is perpendicular to the mid-passage line. The span-width contours in their former axisymmetric case were parallel to the fictitious line between two adjacent blade leading edges. The aerodynamic loss is reduced by a large amount in the mid-span near the flat endwall. Conversely, the loss is increased near the profiled endwall due to the flow separation at the corner of the suction surface and the endwall. Lastly, the three-dimensional effect of the nonaxisymmetric profile resulted in a twist in the blade wake.

Atkins [2] studied experimentally the effect of endwall profiling on secondary losses in a linear turbine cascade. Both two-dimensional (axisymmetric) and three-dimensional (nonaxisymmetric) profiles were tested. One of the two different types of nonaxisymmetric profiles had a bump at the pressure surface near the trailing edge and had a zero height at the suction surface. Conversely, the other nonaxisymmetric case had a bump at the suction surface and

zero height at pressure surface. There was a linear variation between suction and pressure surfaces across the passage. Although the first profile decreased the pressure at the pressure surface, it caused a negative loading at the trailing edge. Similarly, the second profile achieved to lower the pressure gradient at some portion of the passage, but resulted in a pressure rise near the trailing edge. Both profiles increased the loss and the wake was twisted.

Rose [3] aimed to remove the nonaxisymmetric static pressure distribution at the nozzle guide vane (NGV) exit by using contoured hub endwall. The design methodology was to use streamline curvature. Convex curvature (bump) would be used to accelerate the flow and concave curvature (trough) would be used to decelerate the flow locally. There were four profiles tested, one of them was the standard endwall. There were two different shapes in this profile. One in the circumferential direction and the other in axial direction. Circumferentially, a sinusoidal shape was chosen due to the fact that the static pressure non-uniformities after the trailing edge were also sinusoidal. To design the axial shape, a parabola and a sinusoid were joined. The three-dimensional viscous computational fluid dynamics (CFD) code was used to examine the effects of nonaxisymmetric endwalls. A 70% reduction was achieved in the circumferential non-uniformities of static pressure at the NGV exit. The NGV passage flow field came out to be nearly the same as the standard endwall for all types of configurations. The calculated losses for all cases were close and around 3.9% of the total pressure.

Harvey et al. [4] designed a nonaxisymmetric endwall profile for a turbine rotor blade in a linear cascade arrangement. The aim of the study was to reduce secondary flows and the exit flow deviation. The idea was the same as Rose [3] such that streamline curvature was used to control the static pressure field. The newly designed endwalls were examined computationally using a 3D Reynolds Averaged Navier-Stokes (RANS) CFD program. The design of the endwall was done by the product of two curves, one in circumferential and the other in axial direction. B-spline was used at six control points in the axial direction and first three terms of Fourier series were used in the circumferential direction. Two endwall profiles were tested. First study was having convex curvature near the pressure side and concave curvature near suction side. Passage vortex turned out to be smaller. On the other hand, 2 degrees increase in overturning was calculated because of the reduced cross-passage flow. In order to compensate for this problem an extra profiling at the trailing edge was designed in the opposite way (*i.e.* having a trough at pressure side and a bump near the suction side). This design increased the crossflow, as expected. The overturning was reduced 3 degrees when compared to planar endwall. The angle deviation was lessened from 12 to

8 degrees. There was also a total reduction of 40% in secondary kinetic energy. The negative effect of decreasing the overturning was a formation of counter vortex, which was creating another loss system.

A different approach was proposed by Hartland & Gregory-Smith [5] for the design of nonaxisymmetric endwall contouring. The argument was to use vertically offset camberline in the axial profiling. The idea behind this concept originated from the fact that the curvature of the blades caused the secondary flows and using this curvature as an axial contouring profile might help to reduce its effects. The camberline was first rotated about the trailing edge and scaled to have a distance equal to axial chord. For a smooth transition from the axial profiling to the flat endwall, fillets were inserted both at the upstream and downstream joining locations. Next, this profile was offset vertically. The circumferential profile was a half-cosine wave, having maximum height near pressure surface and minimum height near suction surface. First two endwall contours were restricted within the blade passage. Circular fillets were used at the leading edge and trailing edge regions for smoothness. In the third design, a parabola was used for the transition, which was extending upstream and downstream of the passage. CFD results showed a 6% reduction in secondary loss and 61% reduction in secondary kinetic energy coefficient. Authors also noted that the prediction of loss might not be very accurate due to CFD modeling.

Nagel & Baier [6] aimed to rise the efficiency of the turbine NGV by developing a combined design of both vanes and the endwall. A three-dimensional optimization technique was used. A 3D compressible transitional RANS solver was used for the flow simulation. The axial endwall profile was designed by using two spline elements controlling the shape of the endwall. The change in axial profile was also affecting the shape of the vanes. Circumferential profiling was made up of a product of two functions. Between the suction side and the pressure side, a shape function was defined, giving the curvature. The other was the decay function, defined at the pressure and suction sides of the blade on the hub, restricting the endwall profile in the row. The optimized geometry was also tested experimentally. The overturning was reduced and the angle deviation was smaller. There was a total loss reduction of 22% in total pressure and 60% in secondary kinetic energy (SKE).

Saha & Acharya [7] performed 3D computational simulations of a nonaxisymmetric endwall design to reduce the total pressure loss and compare the heat transfer results with the standard endwall. The nonaxisymmetric endwall was created by the product of two curves, one in circumferential and the other in streamwise direction, and then scaling them. The idea was to have concave curvature near the suction surface to increase the local static pressure, and to have convex curvature near pressure surface to decrease local static pressure. There were four different types

of streamwise profiles tested, with a constant circumferential curve. The comparison with the standard endwall was made with the contoured endwall profile which had a measurable heat transfer reduction. Secondary flow vorticity size and strength and the cross-passage pressure gradient were reduced. The heat transfer was decreased near leading edge and in the flow passage (locally 15-20%). At the endwall the area-averaged Nusselt number ( $\text{Nu}$ ) was reduced by 8%. One of the goals which was to minimize the total pressure loss was achieved by 3.2% in mass-averaged values at the downstream of the blade passage.

An alternative nonaxisymmetric endwall profiling was suggested by Torre et al. [8]. In that study, besides the modulation of cross-passage flow, they tried to control the formation mechanisms of horseshoe vortex. Both experimental and computational work was performed. A non-linear unstructured parallel viscous flow solver was used. The nonaxisymmetric profile was designed in such a way that it had the first three terms of Fourier series in the circumferential direction, giving perturbations to the planar endwall surface. In axial direction, there were 6 locations where these perturbations were defined, all having negative deviations. The profile extended from 25% axial chord upstream to 75% downstream of airfoil leading edge. Experimental results showed an achievement of 72% reduction in SKEH (defined as  $SKEH = (\text{Secondary Kinetic Energy}) \cdot \text{Helicity}$ , where  $\text{Helicity} = \vec{\omega} \cdot \vec{V}$ ) and 20% in mixed-out losses as defined in [8]. The cross-passage vortex was weakened. Although CFD overestimated the secondary flows for contoured endwall and underestimated for planar endwall, still it reflected the reduced SKEH and mixed-out losses with profiled endwall.

Nonaxisymmetric endwall contouring was applied to three different turbine blades by Praisner et al. [9]. One blade was a conventional-lift design and the other two were high-lift designs. A 3D structured RANS flow simulation was performed and it was compared with the experimental data. The goal was to minimize the total loss. Gradient-based optimization technique was carried out with the CFD code. The endwall profile was designed with the help of 2D cubic splines both in circumferential and the streamwise direction. Five control points were used circumferentially and axially. They did not restrict the splines to be sinusoidal in circumferential direction, so the flexibility in generating different types of surfaces was increased in the optimization process. However, to keep the flow passage area constant, a throat area correction was added. The measured total loss reduction was 25% for high-lift airfoil and 10% for conventional-lift airfoil. The computational results were around the half of the measured values for both cases. CFD was said to capture the flow tendency, but, it underestimated the total loss.

The specific endwall contours generated throughout this study are based on the minimization of the cross passage endwall static pressure gradient. The specific location of the hills and valleys in this study was chosen to relatively decelerate the near suction side flow in the vicinity of the endwall surface. Attention was also paid to relatively accelerate the endwall flow system near the pressure side where cross flows are strong. Although a completely automated optimization study was not performed at this stage, an intuition based geometry generation approach was in place. Past secondary flow and cross flow generation knowledge was essential in the preparation of the new endwall geometries.

Although endwall contouring provides an overall improvement in existing turbomachinery systems using cylindrical endwalls with only axial contouring, the contribution of nonaxisymmetric endwall contouring could be more substantial in modern turbine designs. In more contemporary systems with reduced blade count, nonaxisymmetric contouring is a way of reducing aerodynamic losses generated near the endwall surfaces. The inherent penalties imposed by reduced blade count can be counteracted by nonaxisymmetric contouring.

This paper will introduce and discuss the specific nonaxisymmetric endwall contouring design methodology used at the Turbomachinery Aero-Heat Transfer Laboratory. Various contoured endwall designs will be presented. The most encouraging one will be selected and analyzed in detail using computational fluid dynamics tools. The NGV flow system under investigation is from the single stage turbine research facility AFTRF described in [10] [11] [12] [13] [14] [15].

## II. Endwall Design Methodology

In the present study, the contoured endwalls are designed in two steps:

- Creating Fourier series based splines at different axial locations on the cylindrical endwall surface. These splines will define a basis for the contoured endwall surface in the circumferential direction.
- Importing these splines to solid modeling program. These circumferentially defined splines will be combined with the help of B-Splines in the streamwise direction.

### A. Spline Generation

The splines are generated at different axial locations of the turbine nozzle guide vane. The methodology of using Fourier series is very similar to the one described in Harvey et al. [4]. Using the first three terms of the Fourier series expansion, one can properly define curves which are useful for endwall contouring purposes:

$$r = \frac{1}{K} \sum_{i=1}^3 \left[ a_i \sin\left(\frac{2\pi L}{p/i}\right) + b_i \cos\left(\frac{2\pi L}{p/i}\right) \right]$$

where  $r$  is the radius of the spline from the axis of rotation,  $K$  is the scaling coefficient (to eliminate a probable shift between the contoured endwall spline and the planar endwall circumferential line),  $a_i$  and  $b_i$  are the Fourier series coefficients,  $L$  is the circumferential distance from the reference point, and  $p$  is the circumferential distance measured between the two blades. MATLAB is used in the final generation of these splines.

## B. Solid Modeling Approach for Final Endwall Definition

The second step in endwall contour generation is to import the previously created endwall splines into the solid modeling program. Throughout this study, Siemens PLM Software NX5 is used as the solid modeling program. The splines, which are already defined in MATLAB at different axial locations, are transferred by the program. Next, the solid modeling program creates a contoured surface with the help of B-Splines to combine these imported splines. The red lines in Figure 1a are the different axial locations where the contoured endwall splines are generated. Leading edge view of the blade passage can be seen from Figure 1b. As before, red lines represent the axial circumferential lines, and the green lines are the imported splines. Then, the solid modeling program combines these splines and creates the contoured endwall as shown in Figure 1c and Figure 1d. For this specific design, the contouring is restricted in the blade passage only, *i.e.* the contouring does not extend in the upstream of the leading edge or downstream of the trailing edge.

In the present study, eight different nonaxisymmetric endwalls are generated and computationally evaluated. Top view of these designs are shown in Figure 2. Contour lines are representing the radius from the axis of rotation in percentage of the blade span. Red regions (bumps) indicate hills, and conversely the blue regions show valleys (troughs). The maximum height of hills or depth of valleys are around 6% of the NGV span. The first seven designs are restricted only in the NGV passage, and the last one is extending in the upstream direction of the leading edge, as seen in Figure 2h.

## III. Computational Details

The computational evaluations of the nonaxisymmetric endwall contour designs are accomplished by the three-dimensional finite-volume flow solver ANSYS CFX. The steady-state, viscous flow simulations are performed for an annular NGV passage, without including the rotor section. There are 23 NGVs and 29 rotor airfoils on the Axial

Flow Turbine Research Facility (AFTRF) at Turbomachinery Aero-Heat Transfer Laboratory of the Pennsylvania State University. The details of the experimental facility is provided in [12] [13] [14] [15].

The computational domain extends one midspan axial chord in the upstream direction, where the experimental inflow conditions are imposed. The circumferentially averaged total pressure and turbulence kinetic energy distribution along the span are specified at the inlet boundary according to the previous experimental research [15]. The outflow boundary is located two chords downstream of the NGV trailing edge and mass flow rate is set at the outlet. NGV, hub, and casing walls have no-slip boundaries with adiabatic conditions. Only one NGV passage is simulated with rotationally periodic side walls.

Menter's [16] two-equation eddy-viscosity model gives good predictions especially when there is an adverse pressure gradient in the boundary layer. This shear stress transport (SST) model is based on k- $\omega$  turbulence closure formulation. Also, the flow through an NGV passage is transitional, and one should account for the transition effects as discussed in Turgut and Camci [11]. One of the methods to predict the transition is the Gamma Theta model implemented in CFX. This model is based on an empirical correlation and two more transport equations are solved; one for the momentum thickness Reynolds number ( $Re_{\theta t}$ ) at the onset of transition, and the other for the intermittency function ( $\gamma$ ). This model is validated for various transitional flows together with SST turbulence model.

Based on the discussion and the results presented in Turgut and Camci [11], the authors applied a body fitted and block structured mesh to represent the flow field. The three-dimensional computational mesh in this effort is created by GRIDPRO from Program Development Company, LLC. Multi-block, body fitted structured grid gives more accurate flow predictions in comparison to unstructured grid, even though unstructured mesh is easy and quicker to implement for complex geometrical designs. An example of a generated structured grid is shown in Figure 3. This figure shows two consecutive NGV leading edges and a blade-to-blade plane. The structured grid is well adapted to the endwall contouring and the blade surfaces. Since the near-wall grid resolution is the key for the simulation of transitional flows and for capturing the secondary flow formation, the non-dimensional wall distance of  $y^+ < 1$  condition is satisfied everywhere in the domain. A total number of 2 million three-dimensional mesh elements are used in the computational domain. This mesh density gives grid independent results, especially on the total pressure coefficient distribution at the NGV exit. The grid independency assessment on total pressure coefficient is an essential and challenging test for the final quality of the current computational predictions. The grid independency

on “total pressure” is much more challenging than the assessment on “static pressure” since the “total pressure” based assessment requires capturing the aerodynamic losses with reasonable accuracy.

The corner fillets at the junction of the blade and hub endwall play an important role in the secondary flow formation. Therefore, the corner fillets are also taken into account in the geometry and the mesh. The details of predicting NGV viscous flow system under the influence of corner fillets are presented in Turgut and Camci [11]. Note that, the contouring is designed in such a way that it starts from pressure surface corner fillet and ends at the suction surface corner fillet. In other words, there is no geometrical modification on the blade pressure and suction surfaces. The reason for that is to see the sole effect of the endwall contouring without changing the blade load distribution.

#### **IV. Results and Discussion**

The aim of this study is to minimize the losses related to the secondary flows. To achieve this, the influence of contoured endwalls are investigated at the exit of the NGV passage. The mass averaged total pressure coefficient,  $C_{pt}$ , is calculated at the NGV exit plane, which is illustrated in Figure 4. The differences of mass averaged  $C_{pt}$  values between the baseline and the contoured endwalls are listed in Table 1. The most encouraging contoured endwall design is the last one, with the contouring extended in the upstream direction. A reduction of 3.2% in loss is achieved at the exit plane. This particular contouring has a similar endwall contouring design concept with [3]. To minimize the passage crossflows, hills are generated near the pressure surface to accelerate the flow and locally decrease the pressure. Valleys are used near the suction surface to decelerate the flow and increase the pressure locally. Consequently, this would help to balance the strong pressure gradient between the pressure and suction surfaces near the endwall surface.

Although this contouring strategy works well, it does not totally eliminate the strong crossflows from the pressure side to the suction side. As listed in Table 1, design D11 has the worst mass averaged  $C_{pt}$  value at the NGV exit. It has two hills, one closer to the pressure side, and the other near the suction side. The hill near the suction side prevents the augmentation of secondary flow due to crossflows to some extent. The core of the secondary flow is found to be closer to the hub endwall than the baseline case. However, the cross passage flow emerging from the pressure side separates from the top of the first hill, and then encounters the second hill. Hence, the total pressure loss due to the flow separation has been risen to the end of the passage. Design D09 has a similar contoured endwall

with two hills, except the amplitudes of the hills are not as tall as D11. The increased total pressure loss for D09 at NGV exit indicates that these specific contoured endwalls with two hills generate extra loss.

D05 has a similar contoured endwall to D14 except the contouring is restricted to the NGV passage. The total pressure loss recovery is not that high as D14. This implies that extending the contouring to the upstream of the NGV leading edge is beneficial for the AFTRF specific contoured endwalls. D07 has the reverse design of D05, with valley near the pressure surface and hill near the suction surface. Again, the hill near suction side lessened the interaction of crossflows and the secondary flow core. But, the authors thought that a design with a valley near pressure side is impractical for endwall cooling purposes.

The contoured endwall designs D12 and D13 have small improvement on total pressure loss at NGV exit. D12 has a hill near the suction surface. It resembles design D07, without a valley near the pressure surface. D13 has a valley near the suction surface minimum pressure point, and has the hill extending from the pressure side to the suction side along the NGV passage. The authors think that a hill closer to the suction side has positive and negative outcomes. The flow separation from the hill reduces the positive effects mentioned in the above paragraphs.

The circumferentially mass averaged total pressure coefficient distribution for design D14 along the span is plotted at the NGV exit plane, in Figure 5. The contoured endwall results are compared to the baseline computational estimation. A comprehensive validation of this baseline simulation with experimental data was accomplished in Turgut and Camci [11], and it was concluded that the baseline results would be used as a basis for contoured endwall design studies. It is clear in Figure 5 that the nonaxisymmetric contouring has an important influence on the total pressure coefficient at the NGV exit. This specific contouring is effective up to 14% span of the vane. Apparently, the  $C_{pt}$  comparison between 7% and 14% show that there is a reduction in the secondary flow loss. On the other hand, below 7% the loss is increased when compared to the baseline. The general picture tells that the secondary flow region is pulled towards the hub endwall. This result is in accordance with [7]. This tendency enhances the interaction of the secondary flow with the hub endwall boundary layer, and hence, increases the losses very close to the wall. Note that, it is important to keep the lossy secondary flow away from the core of the passage, where the streamwise flow velocity components are higher. Weakening the interaction of the secondary flow with the core passage flow results in better mass averaged NGV exit plane estimations of total pressure. In other words, even though the loss is increased close to the endwall, since the velocity magnitudes are lower than the core flow,

the contribution of this loss would be small in computing the mass averaged total pressure loss values for the exit plane.

In addition to the circumferentially averaged comparison, equal contour lines of  $C_{pt}$  are drawn at NGV exit plane as shown in Figure 6. To make a better comparison of these contour lines, additional constant lines are added to the graph. Three circumferential lines (12%, 20%, and 50% span locations) and two almost vertical lines (constant  $y$  lines) are included for reference. The first obvious observation is that the width of the secondary flow region is decreased in size, becoming more compact, as seen Figure 6b. Moreover, the core of the secondary flow is closer to the endwall, in accordance with the discussion on the circumferentially averaged distribution. For the baseline case, the secondary flow core is located around 6.3% span, while for the contoured endwall case the core is around 4.4% span location. The lossy region is pulled towards the hub endwall. As a result, the secondary flow is not as distinct as was in the baseline, and having more interaction with the endwall boundary layer. This can be confirmed from the lower-left corner of the secondary flow area. One other observation to mention is that there is a slight change in  $C_{pt}$  in the core of the wake near the 50% vane span. A decrease of  $\Delta C_{pt} = 0.2$  is achieved on the contoured endwall calculation.

The major effect of nonaxisymmetric endwalls having hills near pressure side and valleys near suction side is pulling the secondary flow to endwall, as discussed in the previous paragraphs. This tendency is also visible in the vortical behavior of the secondary flow. Figure 7 shows the swirling motion of the flow at the NGV exit. Swirling strength is the imaginary part of the complex eigenvalue of the local velocity gradient tensor as described in [17]. The swirling strength is useful in identifying and differentiating the local vortices. The comparison between baseline and contoured endwall simulation tells that contouring has a positive effect in the wake region and also near 9% span location. In the wake and the core of the secondary flow area, the swirling strength magnitude is reduced by 30% and 10%, respectively. The main vortical structure in the secondary flow region is found to be closer to the hub. Note that, the baseline secondary flow was bounded by two vertical lines, 12% span and hub endwall. The equal contours of  $x$ -component of the vorticity vector are plotted in Figure 8. This is the perpendicular component to the NGV exit plane. Contoured endwall has decreased the level of vorticity closer to the hub endwall. Clearly, reducing the crossflows acting from pressure to suction surface resulted in less vortical area just above the hub. The thickness of the  $x$ -component vorticity region is reduced by 0.2% span. Again, the vortical structures are found to be closer to the hub endwall.

The effect of endwall contouring is investigated locally by plotting the circumferential distribution of static pressure coefficient,  $C_p$ . At four different span locations, 0%, 3%, 6%, and 15%,  $C_p$  variations are shown in Figure 9. Increase in  $y$  coordinate represents the passage from suction side to pressure side. Note that, the secondary flow was bounded between  $y = -0.06m$  and  $y = -0.032m$  as shown in Figure 6. Furthermore, the wake region at 15% span starts from  $y = -0.061m$  and ends at  $y = -0.052m$ , distinguishing the wake location downstream of trailing edge. The definition of  $C_p$  tells that lower values indicate less deviation from reference pressure value. At 15% span location, there is a 5% gain ( $\Delta C_p \approx 0.1$ ) around  $y = -0.055m$ , which corresponds to a value of nearly  $170Pa$ . As we go away from the wake and move in the direction of suction side to pressure side, there is a slight gain of nearly 1.2% in the pressure coefficient. This recovery exists for all four span location distributions. Another observation from these figures is that for 0 and 3% span locations, there is an evident pressure gain near  $y = -0.045m$ . At this location, the endwall boundary layer, secondary flow, and wake is mixed.

This NGV design has an exit flow angle of 70 degrees from the axial direction. The circumferential velocity component has a dominant role in the flow physics. The effect of contoured endwall on circumferential velocity is plotted in Figure 10. At 0.5 and 1% span, the contoured endwall reduced the reversed flow approximately  $10 m/s$  around  $y = -0.053m$ , where the total pressure loss has the highest value. The 1.5 and 3% span  $V_\theta$  distributions show that the magnitude of circumferential velocity is reduced starting from the suction side and through the pressure side. This indicates that the crossflow within the passage is less in contoured endwall compared to baseline computations.

To further analyze the flow within the passage and compare the contoured endwall case with the baseline, streamlines are released from the inlet boundary. The streamlines are illustrated in Figure 11. For both cases, the same rectangular clip is used for the streamline origination; between two constant  $y$  lines and under 1% vane span. The streamlines in Figure 11a follow a nearly straight path until they reach the saddle point and then separated into two legs. The strong pressure gradient affects the suction side leg in a way that they are headed to the suction surface near the minimum pressure point. Then they start rising on the suction surface in the radially outward direction. The pressure side leg directs to the suction surface of the consecutive vane. The yellow ones very close to the endwall are the first to change their path to suction surface. Then the red streamlines follow the yellow ones and hit the suction surface. They go under the suction side leg and push it farther outwards. On the other hand, streamlines in Figure 11b do not follow a straight line from the inlet boundary. Instead, they are deflected towards

the suction surface of the vane from the originating location. Suction side leg tends to turn to suction surface again, but with contoured endwall, it occurs farther downstream when compared to baseline computation. Also, pressure side leg is more attached to the hill on the endwall and follows the streamwise direction till the mid-chord line, and then changes its path to suction surface. Hence, the interaction of pressure side and suction side legs are postponed. Remember that, the pressure side leg and strong crossflows were going under the suction side leg and causing it to rise up on the suction surface. This time, since the suction side leg has less interaction with pressure side leg, the secondary flow region is more closer to the hub endwall. This explains the previous discussion on the pulling down behavior of the secondary flow with contoured endwall.

## V. Conclusions

A specific nonaxisymmetric endwall contouring method is introduced. Fourier series based splines were generated at different axial locations. A solid modeling program combined and blended these splines to finalize the endwall geometry. Eight different contoured endwalls were presented. These designs were computationally tested and compared with the baseline computational result. The total pressure coefficient results at NGV exit plane were listed. The one giving the highest reduction in total pressure loss was analyzed in detail.

There was a reduction of 3.2% in the mass averaged total pressure loss at the NGV exit plane for the design D14. The distribution of total pressure coefficient along the span showed that the secondary flow area found to be closer to the hub in contoured endwall case. The effect of pulling the secondary flow to the hub was also confirmed with the total pressure loss contour plots. The secondary flow width was reduced and the interaction of the hub endwall boundary layer with the secondary flow was increased. As a result, loss values were higher near the hub when compared to the baseline case.

The swirling strength magnitude in contoured endwall case D14 was 10% less than the baseline computations in the secondary flow region at the NGV exit. Contoured endwall was effective in reducing the crossflows from the pressure side to the suction side. It was observed from the  $x$ -component vorticity contours that the level of vorticity magnitude was decreased in the secondary flow area and near the hub endwall.

The circumferential distribution of static pressure coefficient at different radial slices showed a static pressure recovery of nearly 1.2% at the NGV exit. This recovery may reach up to 5% in the wake region. The contoured

endwall also helped to minimize the reversed flow by  $10m/s$  up to 1% span at the wake and endwall boundary layer junction. Moreover, the circumferential velocity component distribution between the suction and the pressure side showed that contoured endwall had smaller  $V_\theta$  from 1% to 3% span, indicating reduced crossflows.

Streamlines released from inlet boundary gave an idea of the flow near the hub endwall. For the contoured endwall case, the pressure side leg followed the passage curvature nicely up to mid-chord position, and then turned its path to the suction surface. Suction side leg hit the suction surface again, but in a farther position than the baseline case. The coalescence of the suction side and pressure side leg is delayed, which resulted in a lower loss prediction.

The current study has the NGV only computation in a rotating HP turbine rig. The rotor-stator interaction and the rim seal cavity flow existing in the rotating turbine research rig are not simulated. The investigation including the rotor-stator interaction and rim seal cavity flow is the topic of a subsequent paper under progress.

The current paper provides a complete description of a specific nonaxisymmetric endwall contouring approach developed for the NGV section of a rotating research facility. The method is directly applicable to actual HP turbine systems.

This study showed that nonaxisymmetric endwall contouring has a potential in decreasing the secondary flow losses. The selected contoured endwall design will be manufactured with the stereolithography technique and installed on the experimental facility. The future work will include the experimental evaluation of this particular contoured endwall and comparison with the computational predictions.

Although endwall contouring provides an overall improvement in existing turbomachinery systems using cylindrical endwalls with axial contouring, the contribution of nonaxisymmetric endwall contouring could be more substantial in modern turbine designs. In more contemporary systems with reduced blade count, nonaxisymmetric contouring is a way of reducing aerodynamic losses generated near the endwall surfaces. The inherent penalties imposed by reduced blade count can be counteracted by nonaxisymmetric contouring.

## VI. Acknowledgment

The authors acknowledge the financial support provided by Siemens Energy Inc. and thank to Dr. Matthew Montgomery, Dr. Prakash Chander, Dr. Michael Crawford, Andrew Lohaus, Anthony Malandra, Ching-Pang Lee,

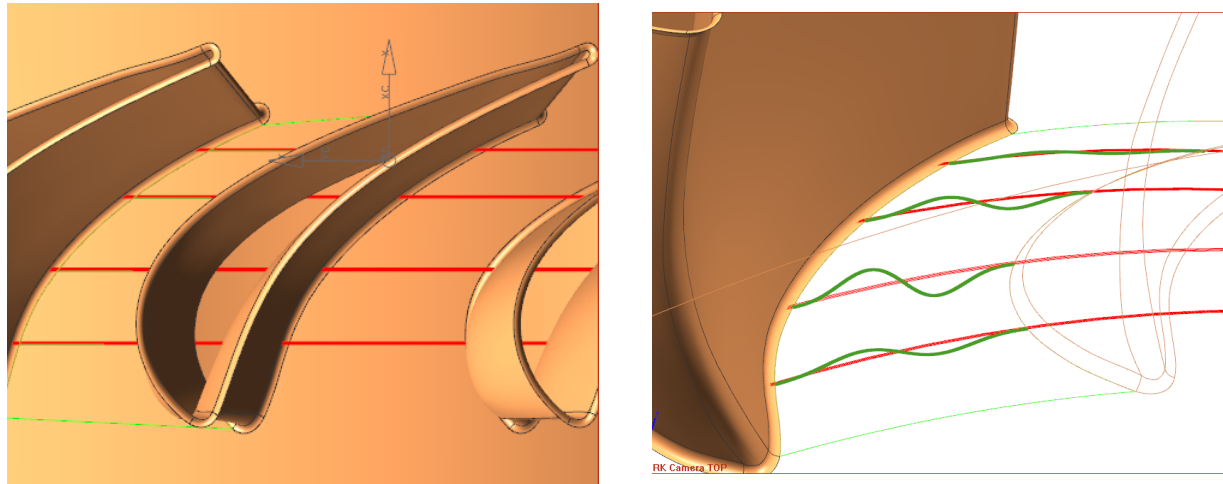
Boris Dobrzynski, Humberto Zuniga, Ken Landis, and Dirk Nuernberger. The authors are thankful to Dr. Ali Akturk for his support during this study.

## Bibliography

- [1] A. W. H. Morris and R. G. Hoare, "Secondary Loss Measurements in a Cascade of Turbine Blades with Meridional Wall Profiling," in *ASME Paper No. 75-WA/GT-13*, 1975.
- [2] M. J. Atkins, "Secondary Losses and End-wall Profiling in a Turbine Cascade," in *The Institution of Mechanical Engineering, Paper No. C255/87*, 1987.
- [3] M. G. Rose, "Non-axisymmetric Endwall Profiling in the HP NGV's of an Axial Flow Gas Turbine," in *ASME Paper No. 94-GT-249*, 1994.
- [4] N. W. Harvey, M. G. Rose, M. D. Taylor, S. Shahpar, J. C. Hartland and D. G. Gregory-Smith, "Nonaxisymmetric Turbine End Wall Design: Part I - Three-Dimensional Linear Design System," *ASME Journal of Turbomachinery*, vol. 122, pp. 278-285, 2000.
- [5] J. C. Hartland and D. G. Gregory-Smith, "A Design Method for the Profiling of End Walls in Turbines," in *ASME Paper No. GT-2002-30433*, 2002.
- [6] M. G. Nagel and R.-D. Baier, "Experimentally Verified Numerical Optimization of a Three-Dimensional Parametrized Turbine Vane With Nonaxisymmetric End Walls," *ASME Journal of Turbomachinery*, vol. 127, pp. 380-387, 2005.
- [7] A. K. Saha and S. Acharya, "Computations of Turbulent Flow and Heat Transfer Through a Three-Dimensional Nonaxisymmetric Blade Passage," *ASME Journal of Turbomachinery*, vol. 130, p. 031008, 2008.
- [8] D. Torre, R. Vazquez, E. de la Rosa Blanco and H. P. Hodson, "A New Alternative for Reduction in Secondary Flows in Low Pressure Turbines," *ASME Journal of Turbomachinery*, vol. 133, p. 011029, 2011.
- [9] T. J. Praisner, E. Allen-Bradely, E. A. Grover, D. C. Knezevici and S. A. Sjolander, "Application of Non-Axisymmetric Endwall Contouring to Conventional and High-Lift Turbine Airfoils," in *ASME Paper No. GT2007-27579*, 2007.

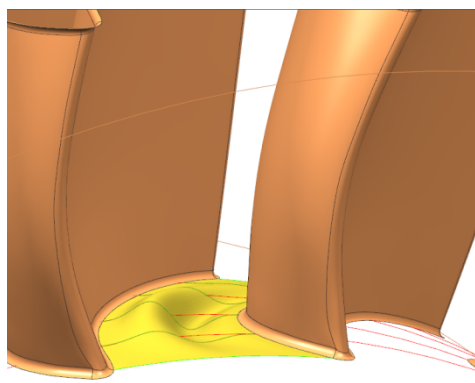
- [10] O. H. Turgut and C. Camci, "A Computational Validation of Turbine Nozzle Guide Vane Aerodynamic Experiments in an HP Turbine Stage," in *ASME Paper No. IMECE2011-64352*, 2011.
- [11] O. H. Turgut and C. Camci, "Factors Influencing Computational Predictability of Aerodynamic Losses in a Turbine Nozzle Guide Vane Flow," *ASME Journal of Fluids Engineering, accepted for publication, September 2015 (A. editor: Frank Visser)*. .
- [12] M. Zaccaria and B. Lakshminarayana, "Investigation of Three-Dimensional Flowfield at the Exit of a Turbine Nozzle," *Journal of Propulsion and Power*, vol. 11, no. 1, pp. 55-63, 1995.
- [13] B. Lakshminarayana, C. Camci, I. Halliwell and M. A. Zaccaria, "Design and Development of a Turbine Research Facility to Study Rotor-Stator Interaction Effects," *International Journal of Turbo and Jet Engines*, vol. 13, pp. 155-172, 1996.
- [14] C. Camci, "Experimental and Computational Methodology for Turbine Tip De-sensitization," *VKI Lecture Series 2004-02 Turbine Blade Tip Design and Tip Clearance Treatment*, 2004.
- [15] M. A. Zaccaria, An Experimental Investigation into the Steady and Unsteady Flow Field in an Axial Flow Turbine, PhD Thesis, The Pennsylvania State University, University Park, PA, 1994.
- [16] F. R. Menter, "Two-Equation Eddy-Viscosity Turbulence Models for Engineering Applications," *AIAA Journal*, vol. 32, no. 8, pp. 1598-1605, 1994.
- [17] J. Zhou, R. J. Adrian, S. Balachandar and T. M. Kendall, "Mechanisms for Generating Coherent Packets of Hairpin Vortices in Channel Flow," *Journal of Fluid Mechanics*, vol. 387, pp. 353-396, 1999.

## FIGURES

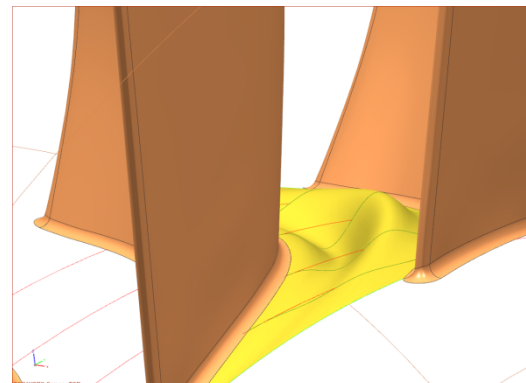


(a) Axial locations where splines are defined

(b) Fourier series based splines in green, circumferential lines in red

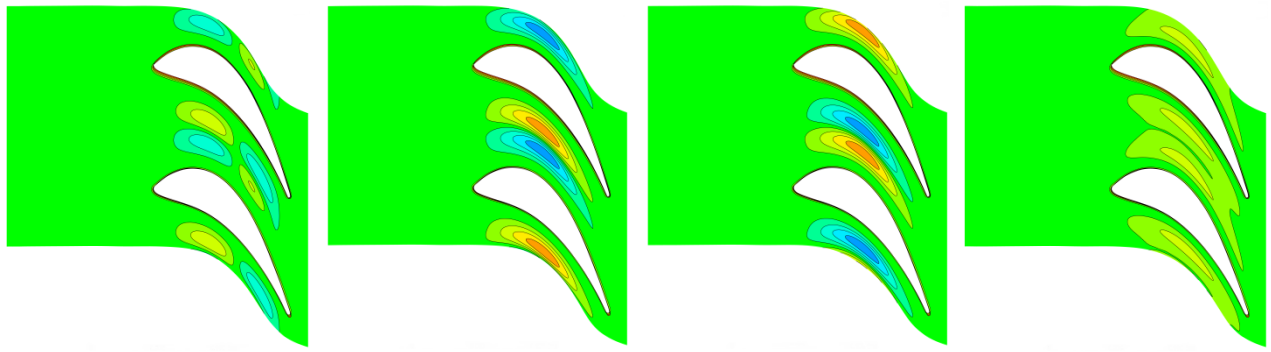


(c) Contoured endwall, leading edge view.

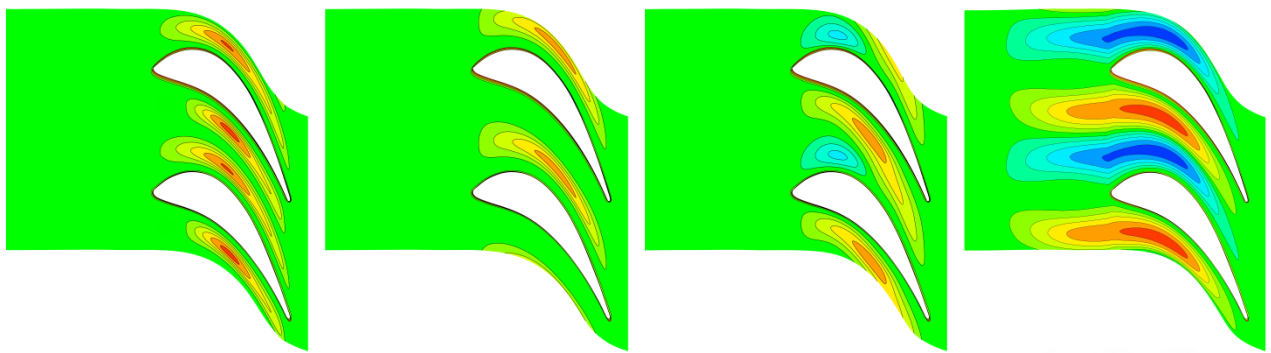


(d) Contoured endwall, trailing edge view.

Figure 1. Use of solid modeling software for endwall contouring.



(a) Contoured endwall, (b) Contoured endwall,  
D04. (c) Contoured endwall, (d) Contoured endwall,  
D05. (e) Contoured endwall, (f) Contoured endwall,  
D07. (g) Contoured endwall, (h) Contoured endwall,  
D09.



(e) Contoured endwall, (f) Contoured endwall,  
D11. (g) Contoured endwall, (h) Contoured endwall,  
D12. (i) Contoured endwall, (j) Contoured endwall,  
D13. (k) Contoured endwall, (l) Contoured endwall,  
D14.

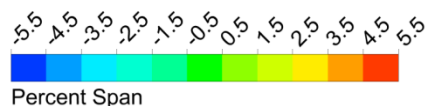


Figure 2. Various nonaxisymmetric endwall contouring designs.

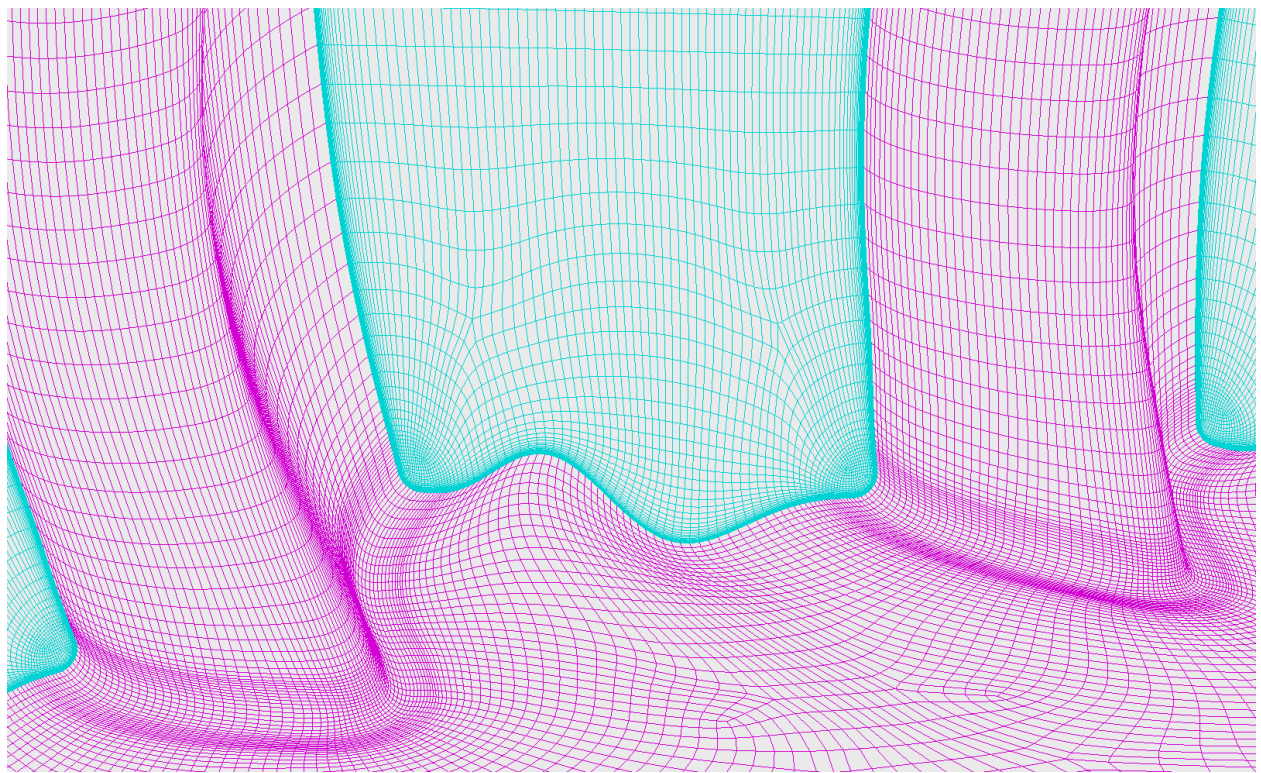


Figure 3. Body-fitted structured mesh with the corner fillets

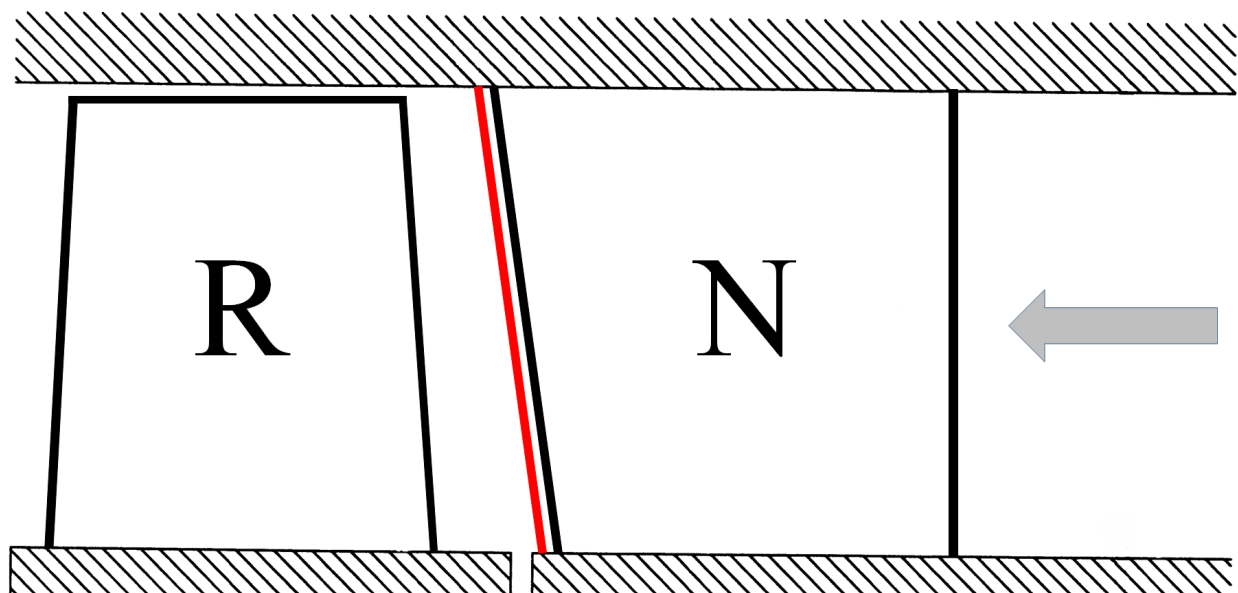


Figure 4. NGV exit plane.

### Circumferentially Mass-Averaged Total Pressure Coefficient

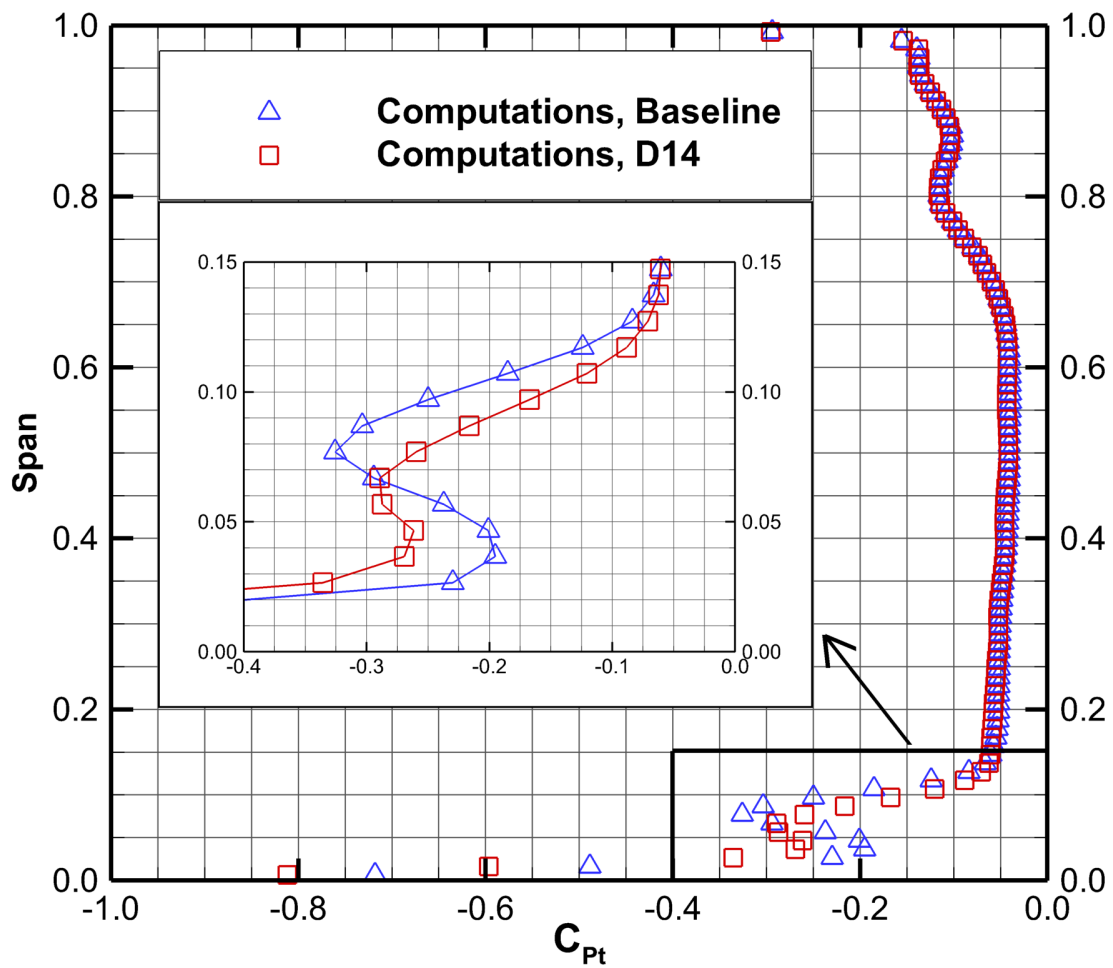
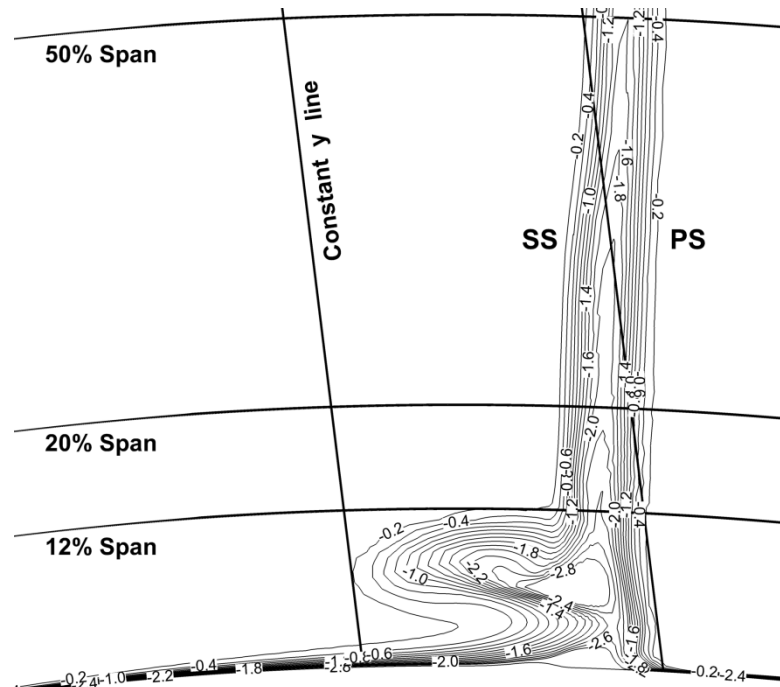
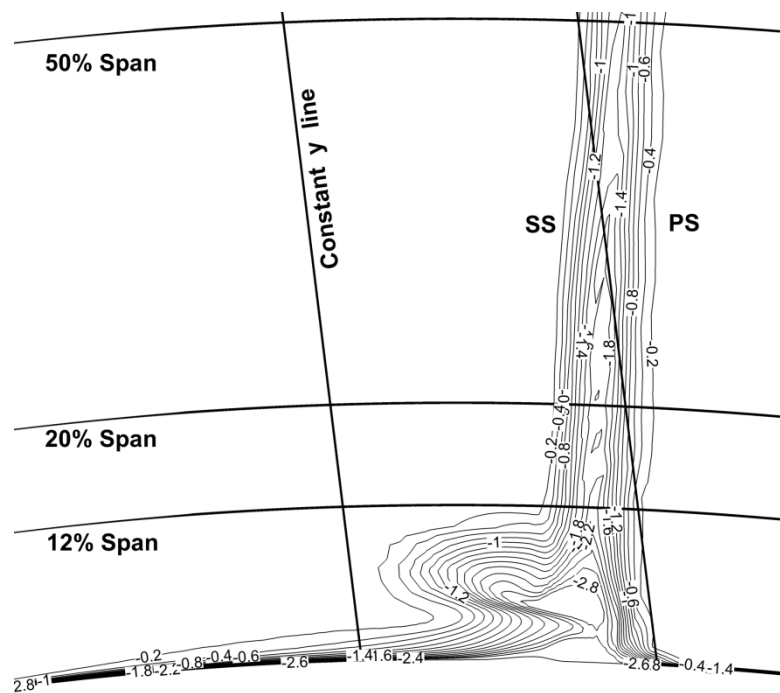


Figure 5. Total pressure coefficient distribution along the span

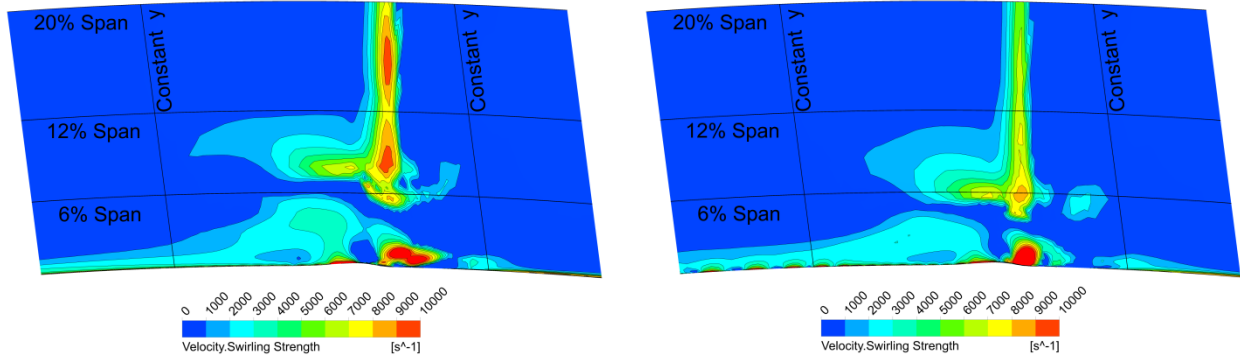


(a) Baseline



(b) Contoured endwall, D14

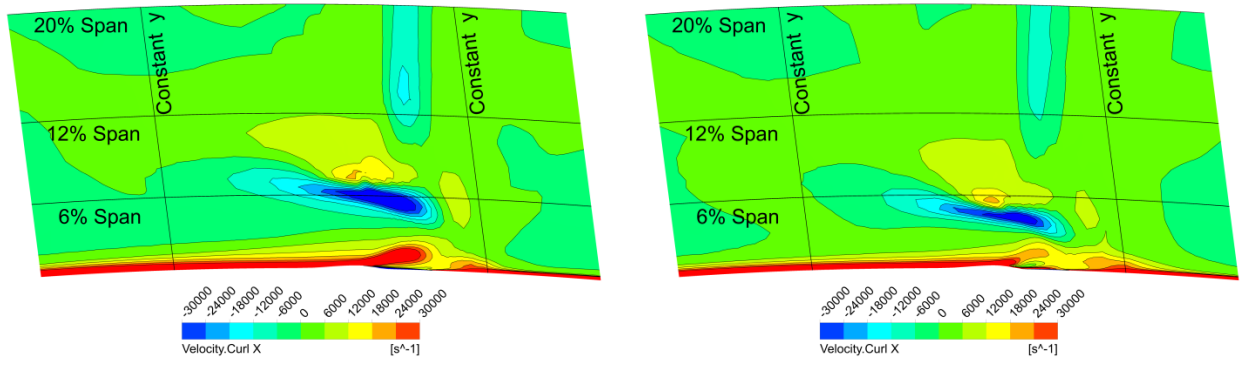
Figure 6. Total pressure coefficient contour lines at NGV exit



(a) Baseline

(b) Contoured endwall, D14

Figure 7. Contours of swirling strength at NGV exit plane.



(a) Baseline

(b) Contoured endwall, D14

Figure 8. Curl of velocity x-component contours at NGV exit plane.

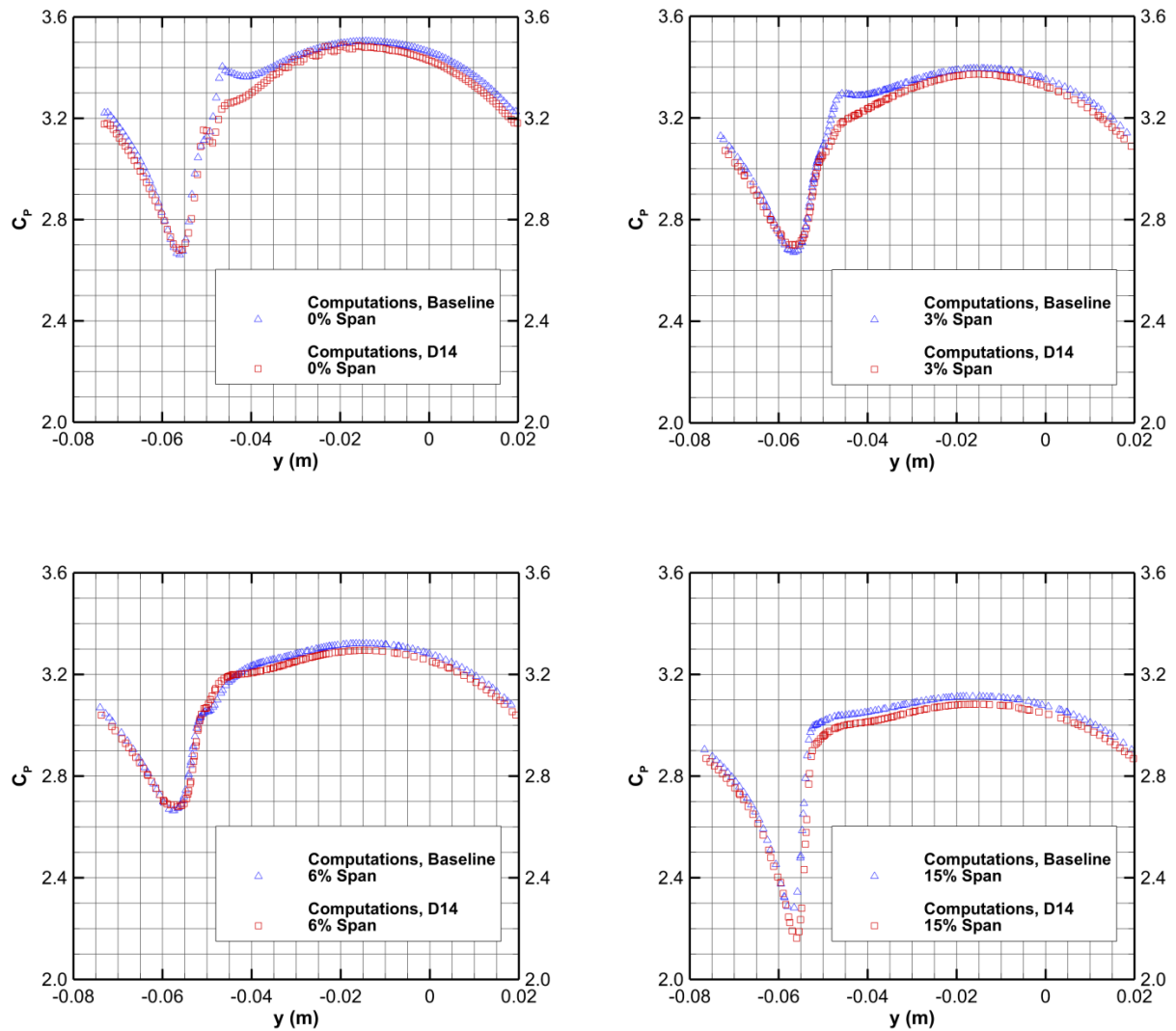


Figure 9. Static pressure coefficient distributions at NGV exit plane.

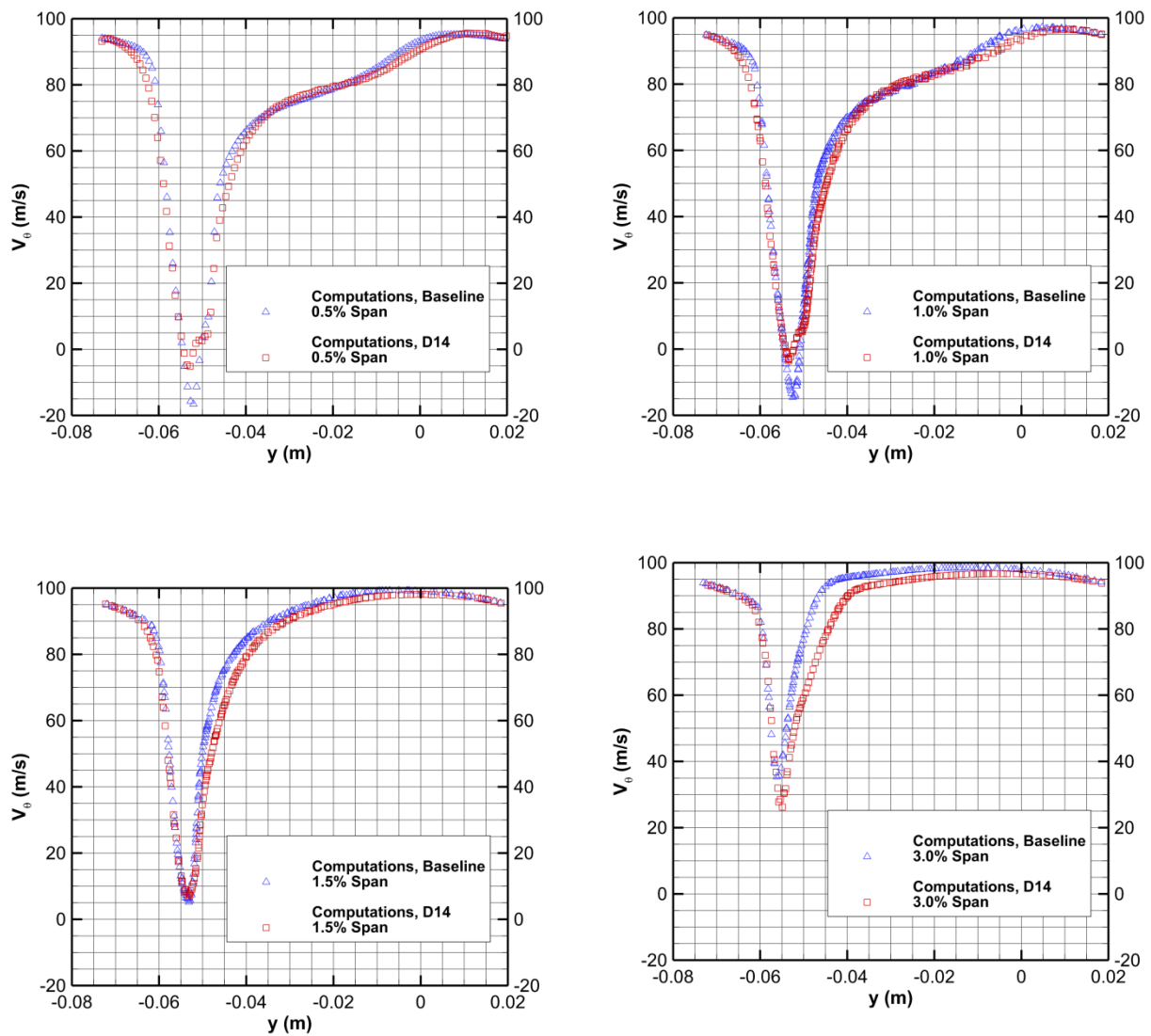


Figure 10. Circumferential velocity component distributions at NGV exit plane.

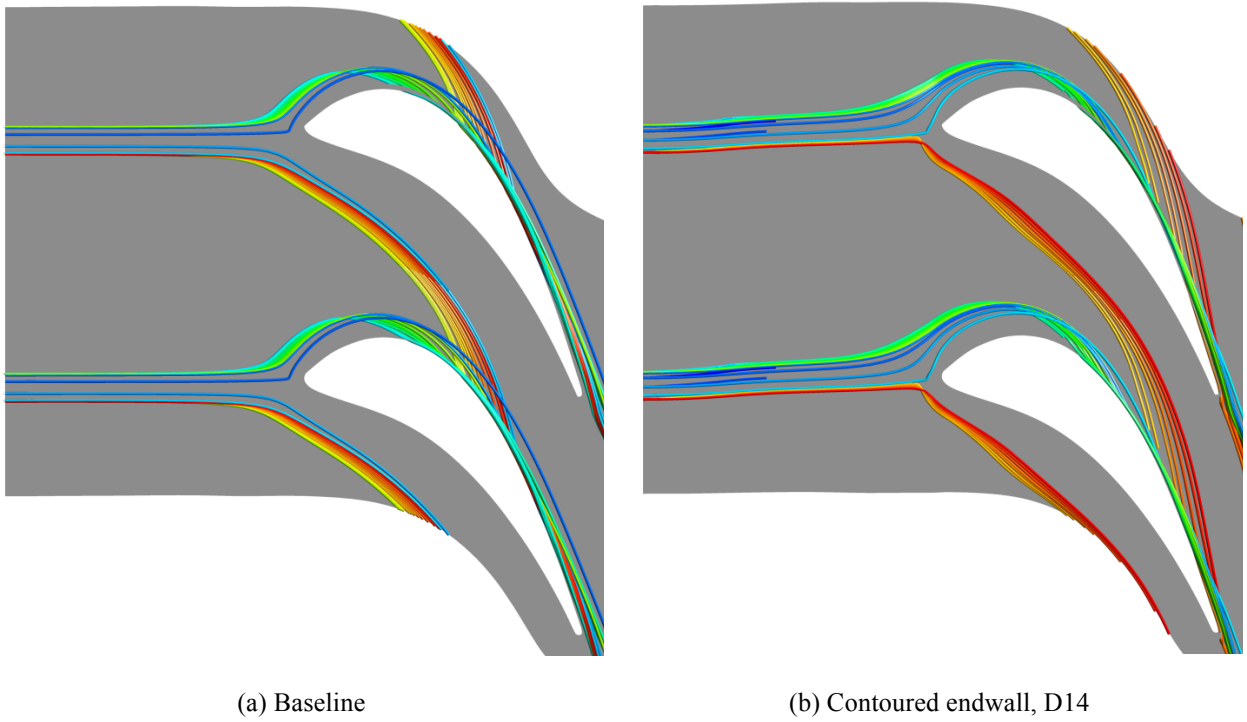


Figure 11. Streamlines released from inlet.

Tables

Table 1. Mass-flow averaged  $\Delta C_{pt}$  estimations at the NGV exit plane.

D04	1.14
D05	1.55
D07	1.52
D09	-0.15
D11	-3.89
D12	0.24
D13	0.27
D14	3.21